Analysis of Disintegration of Planar Liquid Sheet Sandwiched between Gas Streams with Unequal Velocities and Resulting Spray Formation

Sujit Nath[1], Achintya Mukhopadhyay[1,*], Amitava Datta[2], Swarnendu Sen[1]
[1]Mechanical Engineering Department, Jadavpur University, Kolkata – 700032, India
[2]Power Engineering Department, Jadavpur University, Kolkata – 700098, India
sn_ju_mech@yahoo.com, achintya.mukho@gmail.com, sen.swarnendu@gmail.com, amdatta_ju@yahoo.com

Abstract

A temporal stability analysis was carried out for a planar liquid sheet sandwiched between two gas streams moving with unequal velocities. Perturbation analysis was carried out up to second order using the initial amplitude of disturbance of the liquid sheet as the perturbation parameter. Both para-sinuous and para-varicose modes were investigated to determine the dominant break-up mechanism. The nonlinear stability analysis gives the ligament area and the breakup time corresponding to the most unstable wave numbers .Gaster transformation is used to obtain the breakup length from the breakup time. Secondary breakup of the ligament into droplets was modeled following Rayleigh mechanism. Droplet size and velocity distributions were predicted using Maximum Entropy Formulation (MEF). The results show that the asymmetry in the gas velocity significantly affects both the first order and the second order results. The range of unstable wavelengths, the maximum growth rate, the breakup length and the mean droplet diameters were found to be determined through a complex interaction of the gas phase velocities and their differences. It is found that increase in difference the gas velocities on two sides of the liquid sheet leads to a significantly narrower droplet size distribution though the velocity distribution is less affected.

Introduction

Disintegration of liquid sheets has been investigated for the last several decades owing to its importance in spray formation. Excellent reviews on the subject have been provided by Lin and Reitz [1], Lasheras and Hopfinger [2], Sirignano and Mehring [3] and Lin [4]. Although a majority of the studies are limited to linear stability analysis (e.g., [5, 6, 7, 8]), linear analysis cannot provide information on parameters like breakup length. Consequently, in the last few years, a number of researchers have addressed the nonlinear stability problem. Clark and Dombrowski [9] investigated the instability of a planar liquid sheet in a quiescent gas. They used regular perturbation analysis and retained terms up to the second order. Jazayeri and Li [10] extended the work of Clark and Dombrowski [9] by including terms up to third order. They showed that the inclusion of the third order term can significantly alter the sheet profile at breakup. Unlike these works which considered breakup of liquid sheets in stationary gas, Mitra [11] examined the disintegration of planar liquid sheets in a moving gaseous medium. In addition, he considered both sinuous and varicose modes of perturbation unlike the earlier works, which considred only the sinuous mode. Very recently, Nath et al. [12] analysed the breakup of planar liquid sheets in moving gaseous medium, considering gas phase velocity both higher and lower than the liquid sheet velocity. Their analysis identified certain shortcomings in the formulation of both Clark and Dombrowski [9] and Jazayeri and Li [10]. Their prediction of breakup length using second order analysis closely matched that of the third order results of Jazayeri and Li [10] and Mitra [11] in spite of significant differences in the breakup pattern. Their result also showed that within the range of parameters normally encountered in atomization, both sinuous and varicose modes can dominate. In a follow-up work, Nath et al. [13] combined the nonlinear stability analysis with a maximum entropy based model for predicting droplet size and velocity distribution. This approach enables determination of the spray characteristics in terms of atomizer parameters.

All the above works considered equal velocities of the gas layers on either side of the liquid sheet. Very often annular liquid sheets along with high speed inner gas streams are injected into a nearly quiescent gas pool. This configuration is markedly different from that of the studies reported above where the gas stream velocities were equal on each side. Gretzinger and Marshall [14] present photographic images of the breakup of a flat liquid sheet, exposed to high velocity gas on one side and quiescent gas on the other side. It was reported that asymmerty in the gas velocities stabilize the spray on the lower velocity side. Consequently, larger droplets are generally formed on that side. A temporal instability analysis of an inviscid liquid sheet sandwiched between two gas streams of unequal velocity was first studied by Li [15]. He investigated that for unequal gas velocities,

* Corresponding author: achintya.mukho@gmail.com

two independent modes of instabilities exist, which closely resemble the sinuous and varicose modes observed in the case of equal gas velocities. These modes were termed para-sinuous (when the phase difference between two interfaces is close to zero) and para-varicose (when the phase difference between two interfaces is close to π). According to his linear stability analysis, para-sinuous mode was found to be more unstable than para-varicose mode at large Weber numbers and at lower Weber numbers; the para-varicose mode dominates the breakup process. It was reported that surface tension always has a stabilizing effect whereas viscosity has dual effect depending on the conditions. By analyzing the disturbance energy equation he demonstrated that interfacial pressure fluctuations are responsible for instability of the liquid sheet. He also investigated that for Weber number much larger than unity the growth rate curve of para-sinuous mode has only one local maximum, but for Weber number slightly larger and less than unity there exists two maximum values in the growth rate curve. Among these two, growth rate at the longer wavelength is independent of the viscosity, whereas growth rate at the shorter wave length depends on the viscosity of the liquid. But for the para-varicose mode, there is only one maximum at all Weber numbers. Tharakan and Ramamurthi [16] investigated the breakup of a thin viscous liquid sheet co-flowing with the gas streams with different relative velocity and in presence of both longitudinal and lateral waves over liquid-gas interfaces. They reported that for larger Weber mumber and in presence of lateral wave, para-sinuous made have larger growth rate. But the influence of lateral wave on growth rate in not significant when Weber number is more than 10. Witherspoon and Parthasarathy [17] also investigated the breakup of a viscous liquid sheet co flowing with gas phase in both side having both equal and unequal velocity. They used a linear spatial stability analysis to determine the most unstable wave number corresponding to maximum growth rate.

The above studies were all limited to linear analysis. Only few nonlinear analyses of liquid film subjected to unequal gas velocities have been reported in the literature. Ibrahim and Jog [18] carried out a nonlinear stability analysis for annular liquid fuel sheet subjected to unequal inner and outer gas velocities by a perturbation expansion technique with the initial amplitude of the disturbance as the perturbation parameter. However, they investigated mainly configurations with one stream quiescent. Their studies with both gas streams moving were mostly limited to equal gas velocities.

Although in most practical injectors, the fuel emerges as an annular liquid sheet, a planar sheet can be considered as an idealization of the annular liquid sheet owing to the high ratio of liquid sheet radius to its thickness. The present work considers nonlinear temporal stability analysis of planar liquid sheet sandwiched between two gas streams moving with unequal velocities. The instability analysis predicting the breakup of the liquid sheet is coupled with a stochastic model based on maximum entropy formulation for predicting droplet size and velocity distribution.

Mathematical Formulation

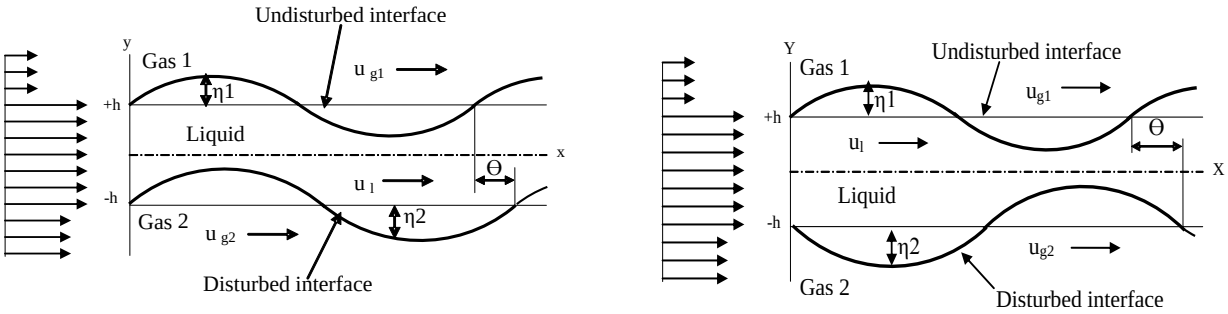

Figure 1 Schematic of plane liquid sheet subjected to para-sinuous (left) and para-varicose (right) disturbance modes

The formulation closely resembles the approach developed in Nath et al. [12]. However, the solution procedure is significantly different and motivated by the approach of Ibrahim and Jog [18]. A schematic diagrams of the present study have been shown in Fig. 1. In the analysis, a steady flow of a two-dimensional planar semi-infinite liquid sheet having density ρ_l, surface tension σ_l and uniform thickness of 2h is considered. The liquid sheet is sandwiched between two inviscid gas steams of density ρ_{g1} and ρ_{g2} and moving with absolute velocities u_{g1} and u_{g2} respectively. The coordinate is chosen such that x axis is parallel to the liquid flow and lies along the centerline of the liquid sheet. As discussed by Li [15] and Tharakan and Ramamurthi [16], in presence of unequal gas velocities, the interface disturbances are neither perfectly sinuous nor varicose. A phase differ-

ence between the two surface waves generated at the two gas-liquid interfaces is represented by Θ. This leads to two modes of perturbation, known as para-sinuous and para-varicose, as shown in Fig 1. A constant velocity field along x direction and zero velocity along y direction are considered as initial condition for the stability analysis. The governing equations, boundary conditions, and initial conditions are similar to Nath et al. [12]

The governing equations for the first and second orders are as follows.

$$\phi_{l1,xx}+\phi_{l1,yy}=0 \quad \text{for} \quad -1\le y\le +1 \tag{1}$$

$$\phi_{g11,xx}+\phi_{g11,yy}=0 \quad \text{for} \quad -1\le y\le +\infty \tag{2}$$

$$\phi_{g21,xx}+\phi_{g21,yy}=0 \quad \text{for} \quad -\infty\le y\le -1 \tag{3}$$

$$\phi_{l2,xx}+\phi_{l2,yy}=0 \quad \text{for} \quad -1\le y\le +1 \tag{4}$$

$$\phi_{g12,xx}+\phi_{g12,yy}=0 \quad \text{for} \quad -1\le y\le +\infty \tag{5}$$

$$\phi_{g22,xx}+\phi_{g22,yy}=0 \quad \text{for} \quad -\infty\le y\le -1 \tag{6}$$

The kinematic boundary conditions for the first and the second order are:

$$\phi_{l1y}-\eta_{11,t}-\eta_{11,x}=0 \tag{7}$$

$$\phi_{l1y}-\eta_{21,t}-\eta_{21,x}=0 \tag{8}$$

$$\phi_{g11,y}-\eta_{11,t}-U_1\eta_{11,x}=0 \tag{9}$$

$$\phi_{g21y}-\eta_{21,t}-U_2\eta_{21,x}=0 \tag{10}$$

$$\phi_{l2,y}-\eta_{12,t}-\eta_{12,x}=\eta_{11,x}\phi_{l1,x}-\eta_{11}\phi_{l1,yy} \tag{11}$$

$$\phi_{l2,y}-\eta_{22,t}-\eta_{22,x}=\eta_{21,x}\phi_{l1,x}-\eta_{21}\phi_{l1,yy} \tag{12}$$

$$\phi_{g12,y}-\eta_{12,t}-U_1\eta_{12,x}=\eta_{11,x}\phi_{g11,x}-\eta_{11}\phi_{g11,yy} \tag{13}$$

$$\phi_{g22,y}-\eta_{22,t}-U_2\eta_{22,x}=\eta_{21,x}\phi_{g21,x}-\eta_{21}\phi_{g21,yy} \tag{14}$$

Similarly, the dynamic boundary conditions for the two orders are:

$$\rho_1\phi_{g11,t}-\phi_{l1,t}+\rho_1U_1\phi_{g11,x}-\phi_{l1,x}=-\frac{1}{We}\eta_{11,xx} \tag{15}$$

$$\rho_2\phi_{g21,t}-\phi_{l1,t}+\rho_2U_2\phi_{g21,x}-\phi_{l1,x}=\frac{1}{We}\eta_{21,xx} \tag{16}$$

$$\rho_1\phi_{g12,t}-\phi_{l2,t}+\rho_1U_1\phi_{g12,x}-\phi_{l2,x}+\frac{1}{We}\eta_{12,xx}=\left(\eta_{11,t}\phi_{l1,y}+\eta_{11}\phi_{l1,yt}\right)-\rho_1\left(\eta_{11,t}\phi_{g11,y}+\eta_{11}\phi_{g11,yt}\right) \tag{17}$$
$$+\left(\eta_{11,x}\phi_{l1,y}+\eta_{11}\phi_{l1,yx}\right)-\rho_1U_1\left(\eta_{11,x}\phi_{g11,y}+\eta_{11}\phi_{g11,yx}\right)+\frac{1}{2}\left(\phi_{l1,x}^2+\phi_{l1,y}^2\right)-\frac{1}{2}\rho_1\left(\phi_{g11,x}^2+\phi_{g11,y}^2\right)$$

$$\rho_2\phi_{g22,t}-\phi_{l2,t}+\rho_2U_2\phi_{g22,x}-\phi_{l2,x}+\frac{1}{We}\eta_{22,xx}=\left(\eta_{21,t}\phi_{l1,y}+\eta_{21}\phi_{l1,yt}\right)-\rho_1\left(\eta_{21,t}\phi_{g21,y}+\eta_{21}\phi_{g21,yt}\right) \tag{18}$$
$$+\left(\eta_{21,x}\phi_{l1,y}+\eta_{21}\phi_{l1,yx}\right)-\rho_1U_2\left(\eta_{21,x}\phi_{g21,y}+\eta_{21}\phi_{g21,yx}\right)+\frac{1}{2}\left(\phi_{l1,x}^2+\phi_{l1,y}^2\right)-\frac{1}{2}\rho_1\left(\phi_{g21,x}^2+\phi_{g21,y}^2\right)$$

Following Ibrahim and Jog [18], the initial conditions for the two orders are:

For para-sinuous mode

$$\eta_{11}(x,0)=\cos(kx);\ \eta_{11,t}(x,0)=0 \tag{19}$$
$$\eta_{21}(x,0)=\cos(kx);\ \eta_{21,t}(x,0)=0$$

For para-varicose mode

$$\eta_{11}(x,0)=\cos(kx);\ \eta_{11,t}(x,0)=0 \tag{20}$$

$\eta_{21}(x,0) = -\cos(kx)$; $\eta_{21,t}(x,0) = 0$

For both modes for the second order

$$\eta_{12}(x,0) = \cos(kx); \eta_{12,t}(x,0) = 0 \qquad (21)$$

$\eta_{22}(x,0) = \cos(kx)$; $\eta_{22,t}(x,0) = 0$

Here $U_1 = \frac{u_1}{u_l}$ and $U_2 = \frac{u_2}{u_l}$, $We = \frac{\rho_l u_l^2 h}{\sigma}$, $\rho_1 = \frac{\rho_{g1}}{\rho_l}$, $\rho_2 = \frac{\rho_{g2}}{\rho_l}$

The perturbation expansion of nondimensional surface disturbance η_j is expressed as

$$\eta_j(x,t) = \eta_0\eta_{j1} + \eta_0^2\eta_{j2} \qquad (22)$$

The first order surface deformation at the upper and lower interfaces can be written in the following forms respectively.

$$\eta_{11}(x,t) = A_1(t)\exp(ikx) + c.c \qquad (23)$$

$$\eta_{21}(x,t) = B_1(t)\exp(ikx) + c.c \qquad (24)$$

Following the solution procedure outlined in [12], the unknown functions in Equations. (23) and (24) can be expressed as $A_1(t) = P_{1a}e^{i\omega_1 t} + P_{2a}e^{i\bar{\omega}_1 t} + P_{3a}e^{i\omega_2 t} + P_{4a}e^{i\bar{\omega}_2 t}$ and $B_1(t) = R_1A_1(t)$ where the constants P_{1a}, P_{1b}, P_{1c}, P_{1d}, and the factor R_1 are not presented here for brevity while $\omega_1, \bar{\omega}_1, \omega_2$, and $\bar{\omega}_2$ are the complex roots of the first order dispersion equation

The second order surface deformation at the upper and lower interfaces can be written in the following forms respectively.

$$\eta_{21}(x,t) = A_2(t)\exp(2ikx) + c.c \qquad (25)$$

$$\eta_{22}(x,t) = B_2(t)\exp(2ikx) + c.c \qquad (26)$$

Following a procedure similar to that in the first order, the second order solution is obtained as

$$\begin{aligned} A_2(t) &= C_{1a}e^{i\omega_{21}t} + C_{2a}e^{i\bar{\omega}_{21}t} + C_{3a}e^{i\omega_{22}t} + C_{4a}e^{i\bar{\omega}_{22}t} + C_{5a}e^{2i\omega_{11}t} + C_{6a}e^{2i\bar{\omega}_{11}t} + C_{7a}e^{(\omega_{11}+\bar{\omega}_{11})t} \\ &+ C_{8a}e^{2i\omega_{12}t} + C_{9a}e^{2i\bar{\omega}_{12}t} + C_{10a}e^{(\omega_{12}+\bar{\omega}_{12})t} + C_{11a}e^{(\omega_{11}+\omega_{12})t} + C_{12a}e^{(\omega_{11}+\bar{\omega}_{12})t} + C_{13a}e^{(\bar{\omega}_{11}+\omega_{12})t} + C_{14a}e^{(\bar{\omega}_{11}+\omega_{12})t} \end{aligned} \qquad (27)$$

$$\begin{aligned} B_2(t) &= C_{1b}e^{i\omega_{21}t} + C_{2b}e^{i\bar{\omega}_{21}t} + C_{3b}e^{i\omega_{22}t} + C_{4b}e^{i\bar{\omega}_{22}t} + C_{5b}e^{2i\omega_{11}t} + C_{6b}e^{2i\bar{\omega}_{11}t} + C_{7b}e^{(\omega_{11}+\bar{\omega}_{11})t} \\ &+ C_{8b}e^{2i\omega_{12}t} + C_{9b}e^{2i\bar{\omega}_{12}t} + C_{10b}e^{(\omega_{12}+\bar{\omega}_{12})t} + C_{11b}e^{(\omega_{11}+\omega_{12})t} + C_{12b}e^{(\omega_{11}+\bar{\omega}_{12})t} + C_{13b}e^{(\bar{\omega}_{11}+\omega_{12})t} + C_{14b}e^{(\bar{\omega}_{11}+\omega_{12})t} \end{aligned} \qquad (28)$$

The constants C_{1a}, $-C_{14a}$, and C_{1b}, $-C_{14b}$, are again skipped for brevity while $\omega_{21}, \bar{\omega}_{21}, \omega_{22}$, and $\bar{\omega}_{22}$ are the roots of the second order dispersion equation.

The nonlinear stability analysis gives the ligament area and the breakup time corresponding to the most unstable wave numbers in para-sinuous and para-varicose modes. The mode for which a lower breakup time is predicted is adopted as the dominant mode and used for further analysis. Gaster transformation is used to obtain the breakup length from the breakup time. Secondary breakup of the ligament into droplets was modeled following Rayleigh mechanism.

Droplet size and velocity distributions are predicted using Maximum Entropy Formulation (MEF). In the MEF approach, the joint size and velocity probability distribution that maximizes the information entropy subjected to certain constraints was considered the most probable distribution. In the present work, the constraints were based on the conservation of mass, momentum and energy of the liquid drops. Although other forms of constraints have been reported in literature, the present set of constraints has been adopted due to their more widespread use and suitability for developing a model free of empirical inputs. The droplet diameter predicted by the breakup analysis is used as the mass mean diameter in the MEF and the breakup lengths obtained from the stability analysis are used in the constraints relations. The MEF module is identical to that of Ref. [13] and hence not repeated here for brevity.

The maximum entropy principle states that the most likely droplet size and velocity distributions are those which maximize the information entropy (Shannon entropy) of the system subject to the constraint conditions. In a spray, a joint probability function $P_{i,j}$ can be defined to express the probability of a droplet to be in a

size (diameter) class '*i*' and velocity class '*j*', where $P_{i,j} = \frac{\dot{n}_{i,j}}{\dot{N}}$ where, $\dot{n}_{i,j}$ is the number of drops formed per unit time having diameter d_i and velocity v_j and $\dot{N} = \sum_{i=1}^{m}\sum_{j=1}^{k} \dot{n}_{i,j}$ represents the total number of droplets formed per unit time in the spray in the entire size range of $i = 1$ to m and velocity range of $j = 1$ to k. The respective Shannon entropy term for the joint probability function is expressed as $S = -K\sum_{i=1}^{m}\sum_{j=1}^{k} P_{i,j}\ln\left(P_{i,j}\right)$. In the present model, the normalization condition of droplets, mass balance, momentum balance and the total energy balance equations are used as constraints. The final forms of the constraint equations are as follows. The details of the derivation are available in Ref. [13].

Normalization Condition: $Z = \sum_{i}^{m}\sum_{j}^{k} P_{i,j} S_1$ (29)

Mass Balance: $Y = \sum_{i}^{m}\sum_{j}^{k} P_{i,j} D_i^3 S_2$ (30)

where, D_i represents the non-dimensional droplet diameter as $D_i = d_i/d_m$.

Momentum Balance: $X = \sum_{i}^{m}\sum_{j}^{k} P_{i,j} D_i^3 V_j S_3$ (31)

Energy Balance: $V = \sum_{i}^{m}\sum_{j}^{k} P_{i,j} D_i^3 V_j^2 S_4 + \sum_{i}^{m}\sum_{j}^{k} P_{i,j} D_i^3 S_4$ (32)

Here, $S_1 = 1$, $S_2 = 1$, $S_3 = 1 + \frac{1}{2}\rho(U-1)^2 LC_f$ and $S_4 = 1 + \rho(U-1)^3 LC_f$ where L = non-dimensional break-up length (l/h), h =half sheet thickness, C_f = drag coefficient and V_j = non-dimensional droplet velocity (v_j/u_l)**.**

The value of $P_{i,j}$ which maximizes the entropy S under the set of constraints is given by the condition

$$\frac{\partial}{\partial P_{i,j}}\left[S + \lambda_1 Z + \lambda_2 Y + \lambda_3 X + \lambda_4 V\right] = 0 \quad (33)$$

where, λ_1, λ_2, λ_3 and λ_4 are Lagrange multipliers.

The solution of Equation (33), gives

$$P_{i,j} = \exp\left[-1 - \lambda_1 - \lambda_2 D_i^3 - \lambda_3 D_i^3 V_j - \lambda_4 D_i^3 V_j^2\right] \quad (34)$$

Results and Discussion

Experimental studies on planar liquid sheet subjected to unequal gas velocities are not readily available. Successful validation with experiments on breakup and spray formation in planar liquid sheets subjected to equal gas velocities on two sides have been reported in Nath et al. [12, 13] and not repeated here for brevity.

First Order Analysis

Figure 2 shows the dispersion curve for a planar liquid sheet sandwiched between a quiescent layer of gas on one side and a moving gas layer on the other side. The results are in excellent agreement with that of Li [15] and thus validates the present formulation. The results show that for both para-sinuous and para-varicose modes, as the velocity of the moving gas layer is increased from zero, both the growth rate and the range of unstable wave number decreases and reaches a minimum at $U_2 = 1$ and then decreases. At $U_2 = 1$, the gas velocity becomes equal to that of the liquid sheet and Kelvin-Helmholtz instability disappears at that interface. This explains the minimum in the growth rate at $U_2 = 1$. In fact, the growth becomes symmetric about $U_2 = 1$ in the range $0 \le U_2 \le 2$. It is also observed that while the growth rate tends to saturate for the para-varicose mode with increase in U_2, it increases steeply for the para-sinuous mode. A comparison of the two figures shows that the growth for para-sinuous mode is one order of magnitude higher than that of the para-varicose mode. Since this is also observed over most of the parameter range studied, results will be presented for para-sinuous mode only unless otherwise mentioned.

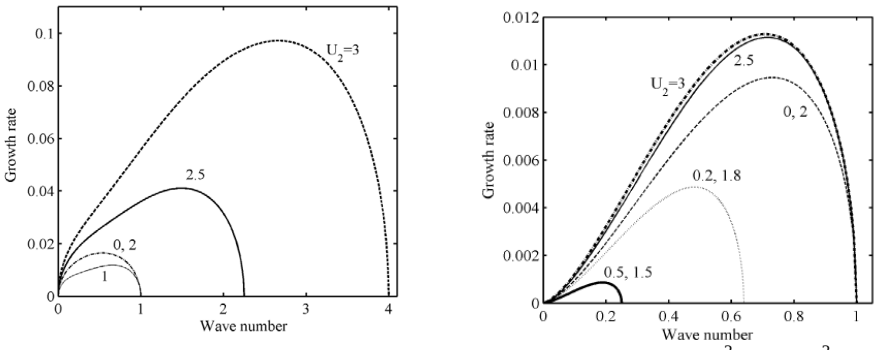

Figure 2 Variation of growth rate with wave number for We = 10^3, ρ = 10^{-3} and U_1 = 0.0 for para-sinuous (left) and para-varicose (right) modes

Figure 3 shows the variation of maximum growth rate and the corresponding critical wave number for para-sinuous mode for different values of U_1 and U_2. The figure shows that both the parameters are primarily determined by the higher velocity. Thus for all the cases at lower values of U_2, both the growth rate and the critical wave number remain largely invariant with U_2. Li [15] had concluded that for liquid sheets with stationary gas on one side, the growth rate was determined by the difference in gas velocities. Since in Li's analysis, the velocity difference was identical to the absolute velocity of the moving gas layer, the present observation is consistent with and a generalisation of the results of Li [15]. Identical growth rates for U_1 = 0 and 2 and the dip at U_2 = 1 are consistent with the observations of Fig. 2.

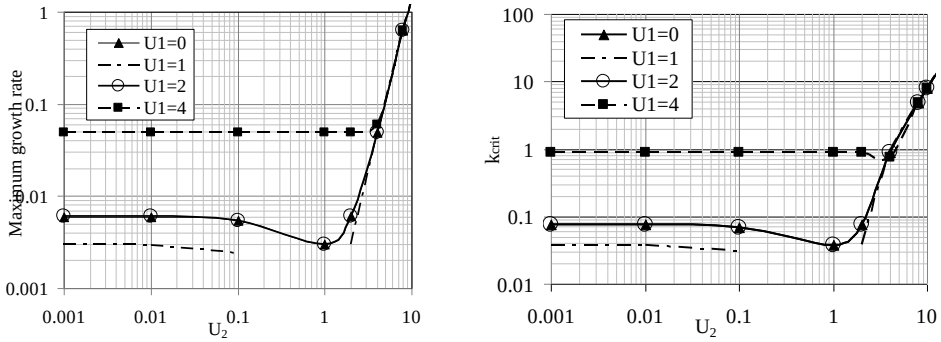

Figure 3 Variation of maximum growth rate and critical wave number for We = 10^3, ρ = 10^{-3} for para-sinuous mode

Second Order Analysis

Figure 4 shows the sheet profiles as predicted by the first order analysis alone and first and second order analyses combined for para-sinuous and para-varicose modes at the respective instants of breakup. As expected, first order analysis alone cannot predict the breakup for the para-sinuous mode. On the other hand, for the para-varicose mode, breakup is predicted by first order analysis at an earlier time than by the combined analysis. The stabilizing influence of the second order was also observed for varicose mode by Nath et al. [12].

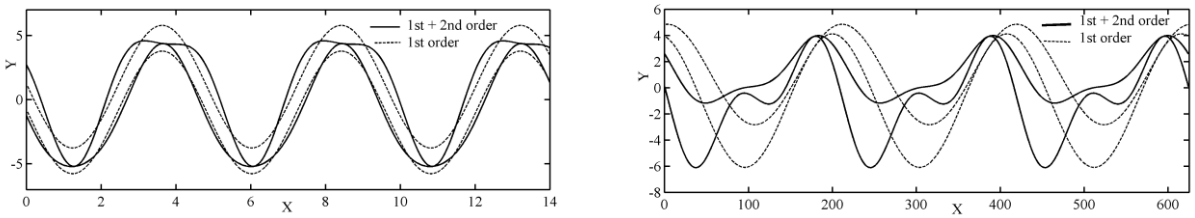

Figure 4 Sheet profile predicted, by first and second order analyses for para-sinuous mode (left) at We=40, U_1=8, U_2=2, ρ=0.001and para-varicose mode (right) at We=40, U_1=4, U_2=1 at instant of breakup

Table 1 shows the effect of the gas velocities on the dimensionless breakup length and ligament areas. The results show a complex dependence on both the absolute values of the gas velocities and the difference between them. For instance, at We = 150 for U_1 =2, the breakup length for U_2 = 0 is lower than that for U_2 = 2, although the total kinetic energy available in the gas phase is higher in the latter case. On the other hand, for U_1=4, the breakup length for U_2 = 2 is higher than that for both U_2 = 0 and U_2 = 4. This effect is more prominent at lower Weber numbers. At We = 150, the ligament area is higher for U_1 = 0 and U_2 =2 than for U_1 = U_2 = 2. However, for U_1 = 4, the ligament size decreases slightly with increase in velocity difference. On the other hand, at lower Weber numbers, the variation of ligament area is similar in nature to that of breakup length. The results are qualitatively different for U_1 =1 owing to the disappearance of Kelvin-Hemholtz instability at one interface.

Table 1: Effect of U_1 and U_2 on breakup length and ligament area

We	U_1	U_2	Dimensionless Breakup Length	Dimensionless Ligament Area
150	1	2	2140.615	163.6246
150	2	2	955.162	83.1109
150	2	4	90.603	7.0518
150	0	2	944.048	83.6643
150	0	4	90.687	7.0274
150	4	4	68.039	8.2663
150	1	4	91.327	6.9805
50	1	2	4572.226	487.0686
50	2	2	2045.315	247.3695
50	2	4	285.457	45.2028
50	0	2	1964.215	246.3994
50	0	4	283.744	44.8479
50	4	4	146.963	27.4255
50	1	4	317.996	48.295
5	1	2	31541.5	4908.739
5	2	2	14786.7	2564.566
5	2	4	1483.626	490.8739
5	0	2	9468.469	2252.038
5	0	4	1412.356	487.0686
5	4	4	734.275	274.3749
5	1	4	1642.154	540.7216

Figure 5 shows the droplet size and velocity distributions for different gas velocities for a fixed value of U_1. As U_2 increases, the droplet size distribution becomes narrower and shifts to smaller size range at all Weber numbers. The velocity distribution becomes more asymmetric and the peak velocity decreases as U_2 increases at We =5. At higher Weber number, the velocity distribution becomes nearly independent of U_2.

Summary and Conclusions

In summary a temporal stability analysis of a plane liquid sheet that is subjected to different non-zero gas velocities on both the sides has been conducted. The effects of density ratio and Weber number on the maximum growth rate for the case of unequal gas velocities are studied. The breakup length is determined by a complex interaction of the absolute values of the gas phase velocities and their difference. Both the droplet size and velocity distributions are affected due to variation in the relative values of the gas streams. Furthermore, Weber number and density ratio of gas to liquid also influence the distributions at different gas stream velocities.

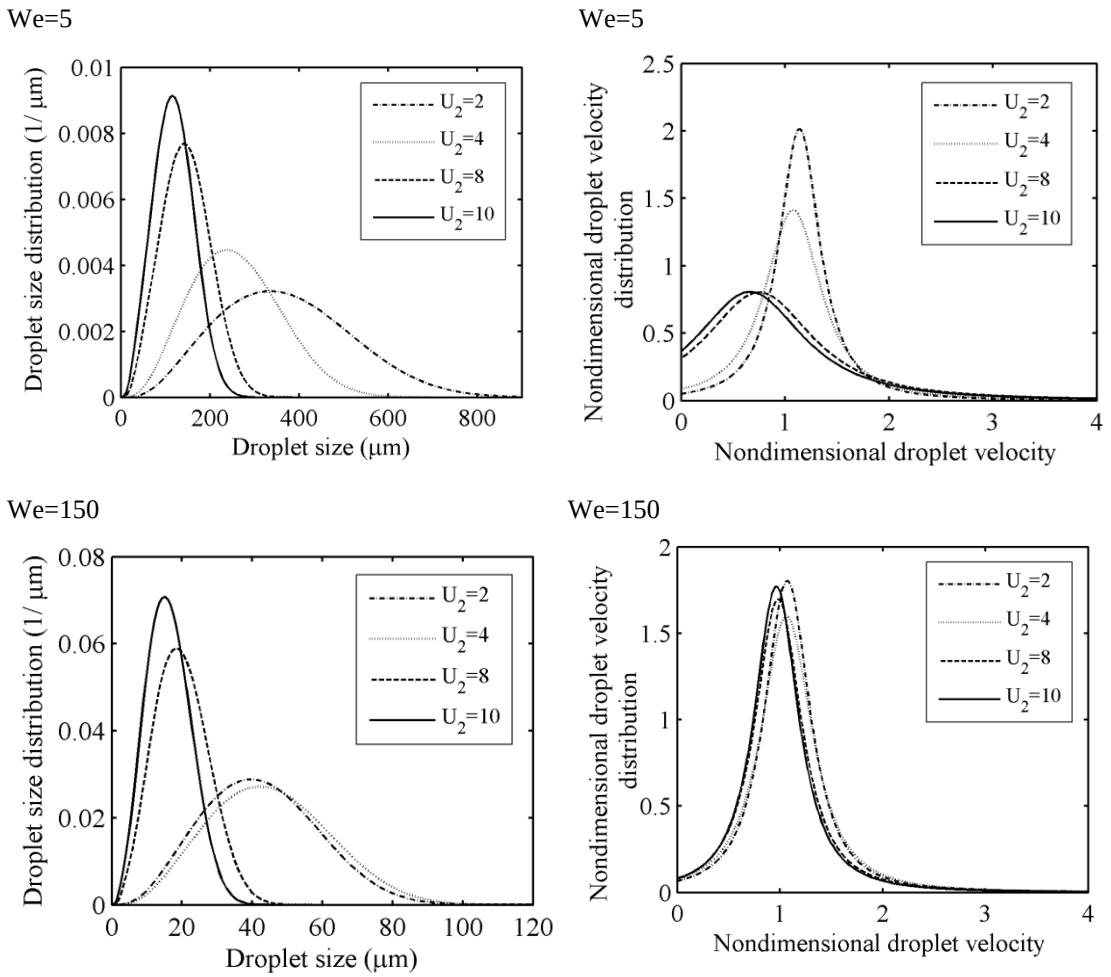

Figure 5 Effect of U_2 on droplet size distribution (left) and droplet velocity distribution (right) for different Weber numbers at ρ=0.001,U_1=4

References

[1] Lin, S.P. and Reitz, R.Z., *Annual Reviews in Fluid Mechanics*, 30: 85 – 105 (1998).
[2] Lasheras, J.C. and Hopfinger, E.J., *Annual Reviews in Fluid Mechanics*, 32: 275 – 308 (2000).
[3] Sirignano, W.A. and Mehring, C., *Progress in Energy and Combustion Science*, 26: 609 – 655 (2000).
[4] Lin, S.P., *Breakup of Liquid Sheets and Jets*, Cambridge University Press, Cambridge (2003).
[5] Squire, H.B., *British Journal of Applied Physics*, 4: 167 – 169 (1953).
[6] Li, X. and Tankin, R. S., *Journal of Fluid Mechanics*, 226:425-443 (1991).
[7] Chuech, S.G., *International Journal of Numerical Methods in Fluids*, 50: 1461 – 1474 (2006).
[8] Rees, S.J. and Juniper, M.P., *Journal of Fluid Mechanics*, 656: 309 – 336 (2010).
[9] Clark, C. J. and Dombrowski, N., *Proceeding of Royal Society London A*, 329:467-478 (1972).
[10] Jazayeri, S.A. and Li, X., *Journal of Fluid Mechanics*, 406: 281 – 308 (1999).
[11] Mitra, S.K., "Breakup Process of Plane Liquid Sheets and Prediction of Initial Droplet Size and Velocity Distribution in Sprays," Ph. D Thesis, University of Waterloo (2001).
[12] Nath, S., Mukhopadhyay, A., Datta, A., Sen, S. and Tharakan,T.J., *Atomization and Sprays*, 20: 983 – 1003 (2010).
[13] Nath, S., Datta, A., Mukhopadhyay, A., Sen, S. and Tharakan,T.J., *Atomization and Sprays*, 21: 483 – 501 (2011).
[14] Gretzinger, J. and Marshall, W. R., *AlChE Journal*, 7: 312-318 (1961).
[15] Li, X., *Acta Mechanica*, 106: 137-156 (1994)
[16] Tharakan, T. J., and Ramamurthi, K., *Atomization and Sprays*, 15: 181-200 (2005).
[17] Witherspoon, W., and Parthasarathy, R. N., *Journal of Energy Resources Technology*, 119: 184-192 (1997).
[18] Ibrahim, A.A. and Jog, M.A., *International Journal of Multiphase Flow*, 34: 647 – 664 (2008).